

# JGR Biogeosciences

## RESEARCH ARTICLE

10.1029/2023JG007438

### Key Points:

- Vegetation, climatic, and soil properties jointly dominated the geographic pattern of soil carbon persistence on a regional and global scale
- Soil depth and forest stand age are important factors regulating the spatial variation of  $\tau_{\text{soc}}$  at global and regional scales
- Our study calls for more efforts on the mechanisms underlying the multiple in driving soil carbon persistence in global forests

### Supporting Information:

Supporting Information may be found in the online version of this article.

### Correspondence to:

L. Yan and J. Xia,  
[lmyan@des.ecnu.edu.cn](mailto:lmyan@des.ecnu.edu.cn);  
[jyxia@des.ecnu.edu.cn](mailto:jyxia@des.ecnu.edu.cn)

### Citation:

Wang, J., Zhu, C., Wei, N., Liu, R., Zhang, B., Chu, C., et al. (2023). Biotic and abiotic factors controlling spatial variation of mean carbon turnover time in forest soil. *Journal of Geophysical Research: Biogeosciences*, 128, e2023JG007438. <https://doi.org/10.1029/2023JG007438>

Received 15 FEB 2023



Accepted 24 JUL 2023

### Author Contributions:

**Conceptualization:** Jianyang Xia  
**Data curation:** Jing Wang, Chen Zhu, Ning Wei, Ruiqiang Liu, Bingwei Zhang, Hongxin Su, Yaozhan Xu, Zhineng Cheng, Sanyuan Zhu, Xugao Wang, Liming Yan  
**Formal analysis:** Jing Wang  
**Funding acquisition:** Jing Wang, Liming Yan, Jianyang Xia  
**Writing – original draft:** Jing Wang, Liming Yan, Jianyang Xia  
**Writing – review & editing:** Jing Wang, Chen Zhu, Ning Wei, Ruiqiang Liu, Bingwei Zhang, Chengjin Chu, Hongxin Su, Yaozhan Xu, Xugao Wang, Liming Yan, Jianyang Xia

© 2023. American Geophysical Union.  
 All Rights Reserved.

## Biotic and Abiotic Factors Controlling Spatial Variation of Mean Carbon Turnover Time in Forest Soil

Jing Wang<sup>1,2</sup>, Chen Zhu<sup>1,2</sup> , Ning Wei<sup>1,2</sup>, Ruiqiang Liu<sup>1,2</sup>, Bingwei Zhang<sup>3</sup>, Chengjin Chu<sup>4</sup>, Hongxin Su<sup>5</sup>, Yaozhan Xu<sup>6,7</sup>, Zhineng Cheng<sup>8</sup>, Sanyuan Zhu<sup>8</sup> , Xugao Wang<sup>9</sup>, Liming Yan<sup>1,2</sup> , and Jianyang Xia<sup>1,2</sup> 

<sup>1</sup>Tiantong National Station of Forest Ecosystem, School of Ecological and Environmental Sciences, East China Normal University, Shanghai, China, <sup>2</sup>Research Center for Global Change and Complex Ecosystems, East China Normal University, Shanghai, China, <sup>3</sup>Zhuhai Branch of State Key Laboratory of Earth Surface Processes and Resource Ecology, Beijing Normal University at Zhuhai, Zhuhai, China, <sup>4</sup>Department of Ecology, State Key Laboratory of Biocontrol, School of Life Sciences, Sun Yat-sen University, Guangzhou, China, <sup>5</sup>Institute of Botany, Chinese Academy of Sciences, Beijing, China, <sup>6</sup>Key Laboratory of Aquatic Botany and Watershed Ecology, Wuhan Botanical Garden, Chinese Academy of Sciences, Wuhan, China, <sup>7</sup>Center of Conservation Biology, Core Botanical Gardens, CAS, Wuhan, China, <sup>8</sup>State Key Laboratory of Organic Geochemistry, Guangzhou Institute of Geochemistry, Chinese Academy of Sciences, Guangzhou, China, <sup>9</sup>Key Laboratory of Forest Ecology and Management, Institute of Applied Ecology, Chinese Academy of Sciences, Shenyang, China

**Abstract** Soil carbon persistence in forests plays a pivotal role in regulating terrestrial feedback to climate change. However, the relative contributions of biotic and abiotic factors in controlling geographic variation of forest soil carbon turnover time ( $\tau_{\text{soc}}$ ) remains unclear. Here, we first sampled soils from 12 permanent forest plots across eastern China and detected higher radiocarbon-derived mean turnover time of soil organic carbon in the deep (30–100 cm;  $2,087 \pm 246$  years) than the surface (0–30 cm;  $249 \pm 80$  years) layer. Further analyses based on the partial Mantel test and structural equation model illustrated that the interactions of climate, vegetation, and soil factors are more complex in deep than surface soils. Then, we established a global database of radiocarbon-derived  $\tau_{\text{soc}}$  from 1897 forest soil samples. On the global scale,  $\tau_{\text{soc}}$  was significantly higher in the deep ( $3,081 \pm 398$  years) than the surface ( $332 \pm 56$  years) layer. Soil depth alone explained 11.7% of the spatial variation in  $\tau_{\text{soc}}$ , and the interactions between climate, stand age, and soil depth account for 68.6% of the variation. These findings highlight the joint control of climate, vegetation, and soil depth in the spatial variation of soil carbon persistence in global forests.

**Plain Language Summary** The soil in the forest ecosystem plays a vital role in modulating feedback between the atmosphere and biosphere under climate change. However, the underlying mechanism of climatic, vegetation, and soil properties regulating soil carbon turnover time ( $\tau_{\text{soc}}$ ) at a geographic scale is still unclear. Here, we established a local data set by collecting soil samples from 12 permanent forest plots in eastern China. The statistical results showed significantly longer  $\tau_{\text{soc}}$  in the deep layer than in the surface layers and different processes at two depths. We then established a global database of forest stand age and radiocarbon-derived  $\tau_{\text{soc}}$ . This study provides fundamental evidence of joint control of climate, vegetation, and soil factors in the spatial variation of soil carbon persistence in global forests.

## 1. Introduction

The soils store most of Earth's terrestrial carbon, so the persistence of soil organic matter is critical for regulating land carbon feedback to climate change (Mathieu et al., 2015; Shi et al., 2020). Forests cover around 30% of the Earth's land area and provide the most significant natural carbon sink to sequester anthropogenic carbon dioxide ( $\text{CO}_2$ ) (Besnard et al., 2018; Bonan, 2016; Friedlingstein et al., 2022). As an essential characteristic of the persistence of organic matter in forest soils, the mean turnover time of soil organic carbon ( $\tau_{\text{soc}}$ ) quantifies the cycling rate of all carbon atoms leaving the soil at a specific time (Schmidt et al., 2011; Sierra et al., 2016). Over a broad biogeographic scale, the climate is often recognized as the primary factor regulating the spatial variation of  $\tau_{\text{soc}}$ . For example, strong negative relationships between  $\tau_{\text{soc}}$  and climate factors, that is, precipitation and temperature, have been detected in both observations (Hein et al., 2020; J. Wang et al., 2019) and Earth system models (Carvalho et al., 2014; Koven et al., 2013). However, the increasing complexity of climate and the rapid change of ecosystems suggested that a single factor can no longer fully explain the spatial variation in  $\tau_{\text{soc}}$  (Van der Voort

et al., 2019). It remains unclear whether and how the biotic and abiotic factors contribute to the spatial variation of  $\tau_{\text{soc}}$  across forest ecosystems on a regional or global scale.

Besides climate, soil properties and vegetation development contribute to soil carbon persistence on a global scale (Heckman et al., 2022; Herold et al., 2014; Shi et al., 2020). Soil properties could determine  $\tau_{\text{soc}}$  by protecting organic matters within aggregates (Torn et al., 1997) or forming chemical associations with minerals (Doetterl et al., 2018). Therefore, either a negative or positive relationship has been observed between  $\tau_{\text{soc}}$  and clay content (Angst et al., 2019; Müller & Höper, 2004), metal-oxides (Doetterl et al., 2015; Khomo et al., 2017), or soil density fractions (Heckman et al., 2022; Trumbore, 1997). Furthermore, all the soil properties mentioned above vary along soil depth (Luo et al., 2019; M. Wang et al., 2022). Compared with the surface layer, soils in the deep layer have older carbon (Shi et al., 2020) and a higher potential for carbon persistence (Trumbore, 2009), with lag in response to climate change (L. Chen et al., 2021). Those observations showed that the dynamic changes of deep soil organic carbon would exhibit different responses compared with surface soil, and its accumulation process may be driven by more specific processes (Kaiser & Guggenberger, 2003; Lützow et al., 2006). Thus, global synthesized evidence suggests that soil depth is an essential predictor of carbon persistence (Heckman et al., 2022; Mathieu et al., 2015). Meanwhile, the changes in aboveground carbon inputs could affect the  $\tau_{\text{soc}}$  as a consequence of the evolution of the forest ecosystem (Ge et al., 2022; Quideau et al., 2001). For example, more fresh carbon inputs from plants and litter can shorten  $\tau_{\text{soc}}$  by stimulating the decomposition rate of soil organic matter (i.e., priming effect; Fontaine et al., 2007). The large global variation in forest age (Curtis & Gough, 2018; McDowell et al., 2020; Poulter et al., 2019) could affect  $\tau_{\text{soc}}$  through changes in plant biomass allocation and litter quality. Sustainable canopy productivity in mature forests has been supported by many direct measurements of forest net CO<sub>2</sub> exchange (Besnard et al., 2018). However, how the carbon cycling rate in soils changes with the developmental stage of vegetation is unclear.

Many studies have emphasized the importance of interactive effects between multiple factors on  $\tau_{\text{soc}}$ . Under continuous changes in aboveground processes, the spatial variation of forest stand age could be a crucial contributor to the biogeographic distribution of  $\tau_{\text{soc}}$ , especially when combined with soil depth. First, forest aging can promote the growth of fine roots in deep soils (Germon et al., 2020), leading to spatial variations in the vertical distribution of fine root traits (Carmona et al., 2021). For example, in-situ observations along forest or soil chronosequence have shown that old forests usually have high fine root fraction (Børja et al., 2008) and specific root length (Holdaway et al., 2011) compared to younger forests. Second, stand age directly influences forest productivity and the carbon allocation among plant organs (X. Chen et al., 2023; Zhu & Xia, 2020), indirectly affecting  $\tau_{\text{soc}}$  by altering the time characteristics of litter carbon inputs. Third, the coupling strength of different chemical elements also depends on soil depth (Qiao et al., 2020). Recent evidence has shown that the physically or chemically formed mineral-organic associations are critical in controlling the spatial variation of subsoil carbon persistence on regional and global scales (C. Chen et al., 2020). Therefore, some Earth system models have recently incorporated dynamics of forest stand age (Nabel et al., 2020) and multiple soil layers (Dai et al., 2019; Koven et al., 2013) to improve the predictions of terrestrial carbon cycling. However, how forest age, soil depth, and their interactive effect with climate contribute to the variation of  $\tau_{\text{soc}}$  over the geographic scale remains not quantified.

Radiocarbon is a powerful proxy to evaluate carbon persistence on long-term timescales (Trumbore, 2009). In this study, we first compiled a global database of radiocarbon-based estimates of  $\tau_{\text{soc}}$ , consisting of 1897 soil samples from 245 forest locations. Then, we sampled soils and measured the radiocarbon signals in 12 permanent forest plots in five mountains across the Eastern Asia monsoon region (20–40°N, 100–145°E, Figure 1 and Figure S1 in Supporting Information S1). The stand ages of the 12 permanent forest plots ranged from 25 to 200 years (Table 1). We also measured soil physical and chemical properties at different depths and biological factors such as litter mass and fine-root biomass. Overall, this study aims to answer two specific questions: (a) How does  $\tau_{\text{soc}}$  vary across forest ecosystems at the geographic scale, and (b) Which biotic and abiotic factors regulate the spatial variation of  $\tau_{\text{soc}}$  in forests?

## 2. Materials and Method

### 2.1. Soil Sampling in Forests Across the Eastern Asian Monsoon Region

We sampled soils from 12 permanent forest plots in five mountains in the Eastern Asian Monsoon region (Table 1, Figure 1 and Figure S1 in Supporting Information S1). Five of the 12 forest plots are members of the

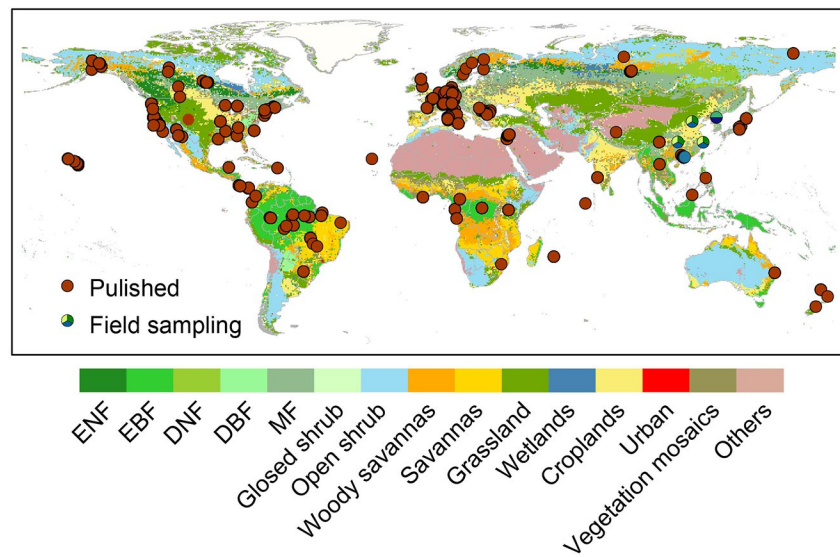


**Figure 1.** Global map showing the location of forest soil organic carbon (SOC) turnover time ( $\tau_{\text{soc}}$ ) based on radiocarbon worldwide. The filled dots in this map indicated published SOC turnover time ( $\tau_{\text{soc}}$ ) based on the radiocarbon method ( $n = 1,897, 1,873$  from literature, and 24 from this study), and the time period of those data ranged from 1958 to 2017. The pie charts in this map indicate the sampling sites along with eastern China. The pie charts with different parts indicated the plots with corresponding different forest ages. The plant functional type is based on the MCD12C1 product classification (Friedl & Sulla-Menashe, 2022).

Smithsonian Forest Global Earth Observatory network (ForestGEO, <https://forestgeo.si.edu/>; Anderson-Teixeira et al., 2018; Chu et al., 2019). The other seven forest plots are members of China's National Ecosystem Research Network (CNERN, <http://www.cern.ac.cn>). In the Eastern Asian Monsoon region, more than half of the total

**Table 1**  
Location and Basic Information Along the North-South Transect of East China

Sampling mountains	Location	Plot	Stand age (year)	Parent materials	Soil taxonomy (USDA)	MAT (°C)	MAP (mm)	PFT
Changbai Mount (CB), Jilin	42.47°N, 128.08°E	Plot 1	200	Basalt and granite	Alfisol	3.3	671	Temperate conifer broad-leaved mixed forest
		Plot 2	80					
Dongling Mount (DL), Beijing	40.01°N, 115.45°E	Plot 3	54	Sand shale, granite	Inceptisols	4.9	570	Warm temperate deciduous forest
		Plot 4	89					
		Plot 5	107					
Tiantong Mount (TT), Zhejiang	29.48°N, 121.47°E	Plot 6	25	Quartzite and granite	Alfisol	16.2	1,375	Subtropical mixed broad-leaved forest
		Plot 7	55					
		Plot 8	120					
Badagongshan Mount (BDG), Hunan	29.65°N, 110.16°E	Plot 9	50	Slate shale, fine sandstone, siltstone, and siliceous rock	Hapludalfs	11.5	2,105	Subtropical mixed evergreen broad-leaved forest
		Plot 10	80					
		Plot 11	100					
Heishiding Mount (HSD), Guangdong	23.86°N, 111.81°E	Plot 12	116	Granite, limestone, and quaternary red clay	Oxisols	19.6	1,744	Subtropical monsoon evergreen broad-leaved forest

Note. MAT, mean annual temperature; MAP, mean annual precipitation; PFT, plant functional type. Soil taxonomy is classified according to the United States soil taxonomy series (USDA, 1996).

annual rainfall occurs in the summer (i.e., June, July, and August) (Tardif et al., 2020; Tian et al., 2003). The soil in site Changbai Mount (CB) is classified as dark brown forest soil (Alfisol, according to the US Soil Taxonomy Series, 1999). The parent materials mainly include granite and basalt. The soil formation process is mainly characterized by weak acid leaching and the humus accumulation process in the temperate humid forest (Zhao et al., 2019). The soil in site Dongling Mount (DL) is classified as brown forest soil (Inceptisols). The major pedogenic process is composed of weathering of sand shale and granite (Fu et al., 2004). The soil in Tiantong Mount (TT) is classified as mountainous yellow and red soil (Alfisols). The substrate of parental material is composed of Mesozoic sediments and acidic intrusive rocks, including quartzite and granite (Yan et al., 2009). The soil in site Badagongshan Mount (BDG) is classified as mountain yellow-brown soil (Hapludalfs) and developed mainly from slate shale, fine sandstone, siltstone, and siliceous rock with a thin mineral A horizon (about 10 cm). The major pedogenic processes are characterized by leaching, clay accumulation, and litter deposition (Li, 2016; Li et al., 2017). The soil in site Heishiding Mount (HSD) is classified as red soil (Oxisols). The parent material is sand shale, limestone, and a small portion of Quaternary red clay (He, 2016).

We estimated the  $\tau_{\text{soc}}$  by the radiocarbon dating analysis of up to 100 cm of soil depth in each forest plot. For each plot, we separated the whole soil increment into the surface (0–30 cm) and deep (30–100 cm) layers to test the radiocarbon signal due to the high financial cost. Details of the location, climate, and vegetation for each sampling site are provided in Table 1, Table S1, and Text S1 in Supporting Information S1. Nine soil cores (2.5 cm in diameter) were collected in each forest plot, and each soil column was separated by a depth of 10 cm from 0 to 100 cm. In total, 108 soil profiles were sampled across the 12 forest plots. The accumulated aboveground litter was collected and measured in an area of 50 × 50 cm in each forest plot, with three replicates adjacent to each soil profile. Fine roots (<2 mm in diameter) were collected by sequential soil cores and manually picked from soil samples. Twelve soil cores were collected randomly in a plot using a soil auger (with an inner diameter of 5 cm and a length of 100 cm). The fine roots were gently picked up with tweezers after being washed off the soil. The fine root biomass of each layer in a plot was averaged by the 12 samplings. The fine root biomass of whole profiles in each sampling plot was added by all depths. The litter and root samples were dried at 65°C for 48 hr using an oven and then weighed for dry mass. The elevation and other geographic information of each forest plot were measured during the soil sampling (Tables S2–S6 in Supporting Information S1).

The soil samples were air-dried in the laboratory and then sieved to 0.15 mm to analyze the contents of soil organic carbon, nitrogen, and phosphorus. Stones and fine roots were separated and weighed before the chemical analyses. The content of soil organic carbon (SOC,  $\text{g} \cdot \text{kg}^{-1}$ ) was measured by dichromate heating-oxidation (Liu et al., 1996). Total nitrogen concentration (TN,  $\text{g} \cdot \text{kg}^{-1}$ ) was determined using the modified Kjeldahl method (Keeney & Page, 1982). Total phosphorus concentration (TP,  $\text{g} \cdot \text{kg}^{-1}$ ) was determined by the molybdenum blue colorimetric method (Murphy & Riley, 1962). The C:N, C:P, and N:P were calculated by the ratio of SOC, TN, and TP, respectively. Soil pH was measured by a pH meter with a soil: water ratio of 1:2.5. The soil cation exchange capacity (CEC) was measured by summing the exchangeable cations, consisting of base and acid cations. The base cations include calcium ( $\text{Ca}^{2+}$ ), magnesium ( $\text{Mg}^{2+}$ ), potassium ( $\text{K}^{2+}$ ), and sodium ( $\text{Na}^{2+}$ ), and the acid cations include hydrogen ( $\text{H}^+$ ), aluminum ( $\text{Al}^{2+}$ ), and ammonium ( $\text{NH}_4^+$ ). The details of climate and other site information can be found in Text S1 and Table S8 in Supporting Information S1. To explore the effects of Al/Fe minerals on  $\tau_{\text{soc}}$ , we analyzed total  $\text{Fe}_2\text{O}_3$  and  $\text{Al}_2\text{O}_3$  in the bulk soil using inductively coupled plasma atomic emission spectroscopy (ICP–AES; Agilent 7500a, USA). Specifically, the soil sieved to 0.15 mm and weighted 0.1 g was fused with 0.7 g lithium metaborate at 1,000°C for 15 min. After cooling, the sample was added to 60 mL 10%  $\text{HNO}_3$  with continuous stirring until completely dissolved. The sample solution was diluted with 5%  $\text{HNO}_3$  into 100 mL prior to further ICP–AES analysis (Liu et al., 1996). The analytical precision is  $\pm 5\%$  for total  $\text{Fe}_2\text{O}_3$  and  $\text{Al}_2\text{O}_3$ . The data set of climatic and site information is also provided by the National Ecosystem Science Data Center, National Science & Technology Infrastructure of China (<http://www.nesdc.org.cn>).

## 2.2. Global Database of Radiocarbon-Based $\tau_{\text{soc}}$

Global soil radiocarbon data was analyzed using the International Soil Radiocarbon Database (ISRaD v.1.0; Lawrence et al., 2020). ISRaD is an open-source data with the records of 8 biomes (i.e., forest, grassland, cropland, shrubland, savanna, tundra, permafrost, and others). Since we focus on the turnover time of SOC ( $\tau_{\text{soc}}$ ) based on radiocarbon occurring in the natural forest ecosystem, so we limited our study to data from soil depth within 200 cm in the forest ecosystem. Radiocarbon is reported in units  $\Delta^{14}\text{C}$  in this study and normalized to the year 2000 (Shi et al., 2020). The positive value of  $\Delta^{14}\text{C}$  indicated the disturbance by nuclear weapons testing

during the 1950s and 1960s, while the negative value of  $\Delta^{14}\text{C}$  indicated that carbon was less affected by nuclear weapons testing. The ISRaD database also collected climatic variables (mean annual temperature, precipitation), soil properties (soil depth, organic carbon content, and clay content), and land cover type. When the information is missing, we collect it from other open databases.

Overall, we combined a database of radiocarbon-based  $\tau_{\text{soc}}$  of 1897 soil samples from 245 forest locations worldwide (Figure 1). It covers a wide geographical range (35.65°S–68.80°N; 159.64°W–173.57°E) and a broad nature climate zone (–12.25 to 27.70°C; 88–6,910 mm) over the half a century (1958–2017). The soil depth was calculated at the midpoint between the top and deep layers of each depth increment. For those works of literature with no description of the site-level climate, we extracted the 30-year average value of (1970–2000) the mean annual temperature (MAT) and precipitation (MAP) from the WorldClim open data sets (<http://www.worldclim.org/>) based on their geographical information. Where forest age is missing, we derived it from the global forest age data set (GFAD v 1.0; Poulter et al., 2019). The GFAD database represents the distribution of forest stand age during 2000–2010 years.

### 2.3. $^{14}\text{C}$ Measurement of Soil Samples

Radiocarbon of bulk soil samples was measured by the accelerator mass spectrometry (AMS) at the State Key laboratory of organic geochemistry, Guangzhou Institute of Geochemistry, Chinese Academy of Sciences, China. Soil samples for radiocarbon analyses were taken with a depth interval of 10 cm along with the soil profiles. We applied the least significant difference (LSD) test to compare differences in SOC turnover time ( $\tau_{\text{soc}}$ ) among different soil depth intervals. The LSD test showed that the topsoil (0–30 cm) had significantly lower  $\tau_{\text{soc}}$  than the subsoil (30–100 cm) (Figure 3b). Thus, we separate two soil increments for radiocarbon dating at each site due to the high financial cost. Two depths (surface layer: 0–30 cm and deep layer: 30–100 cm) were chosen for subsequent analyses and combined accordingly. The soil samples for radiocarbon dating were pre-treated with acid (soaked in 0.1 M HCl for 10 hr) to remove carbonate. The soil samples were washed free of mineral acid with distilled water, dried, and homogenized. It is noted that using acid hydrolysis to remove carbonate in soil samples would create uncertainty in estimating  $\tau_{\text{soc}}$  because of losing soluble organic carbon, which has a lower  $\tau_{\text{soc}}$  (Paul et al., 2001).

The results of the radiocarbon concentrations are given as fraction modern  $F$  and  $\Delta^{14}\text{C}$ , including blank correction and normalization for isotopic to  $\delta^{13}\text{C}_{\text{PDB}} \text{‰} = -25\text{‰}$  (Schoer et al., 2016; Stuiver & Polach, 1977; Torn et al., 2009):

$$F = \frac{A_{\text{SN}}}{A_{\text{ON}}} = \frac{\left( \frac{^{14}\text{C}}{^{12}\text{C}+^{13}\text{C}} \right)_{\text{sample}(-25)}}{0.95 \times \left( \frac{^{14}\text{C}}{^{12}\text{C}+^{13}\text{C}} \right)_{\text{standard}(-19)}} \quad (1)$$

where the  $A_{\text{SN}}$  and  $A_{\text{ON}}$  are  $^{13}\text{C}$ -corrected sample activity and 0.95 times the measured activity of standard normalized to a  $\delta^{13}\text{C}$  of  $-19\text{‰}$  (Stuiver & Polach, 1977).

### 2.4. Radiocarbon-Based Estimation of $\tau_{\text{soc}}$ at the Site Level

In this study, we assume that the soil carbon pool is a well-mixed system with steady-state and atmospheric carbon dioxide as the carbon input ( $I$ ). To determine the mean SOC turnover time ( $\tau_{\text{soc}}$ ), we used a time-dependent model (Gaudinski et al., 2000; Torn et al., 2009) as described by Equation 2. This model is based on several assumptions: (a) the soil carbon pool is homogenous; (b) the rates of carbon input are equal to the output; (c) the time lag between photosynthetic fixation and new carbon input to the soil carbon pool is less than 1 year; and (d) all carbon atoms in the carbon pool have the equal probability of leaving that pool. It is worth noting that the mean SOC turnover time ( $\tau_{\text{soc}}$ ) was equal to the residence time under steady-state (Sierra et al., 2016).

$$F'_{C,t} \times C_t = I \times F'_{\text{atm},t} - C_{t-1} \times F'_{C,t} \times (1 - k - \lambda) \quad (2)$$

where  $I$  represents the carbon inputs in a given carbon pool.  $C_t$  and  $C_{t-1}$  are the carbon content in years  $t$  and  $t - 1$ , respectively.  $k$  is the decomposition rate of SOC.  $\lambda$  is the half-life decay ( $\lambda = 1.21 \times 10^{-4} \text{ year}^{-1}$ ). At steady state,  $C_{t-1} = C_t = I/k$ , and Equation 2 could be further rewritten to:

$$F'_{C,t} = k \times F'_{\text{atm},t} + F'_{C,t-1} \times (1 - k - \lambda) \quad (3)$$

where  $F'_{C,t}$  and  $F'_{C,t-1}$  are represented by the absolute fraction modern of the soil sample in year  $t$  and  $t - 1$ , respectively ( $F'_{C,t} = \Delta^{14}\text{C}/1,000 + 1$ ).  $F'_{\text{atm},t}$  is the absolute fraction modern for the atmosphere carbon fixed in year  $t$ . The

atmospheric radiocarbon curve of the bomb-spike period (1950–2010) was obtained from Northern Hemisphere Zone 1 by Hammer and Levin (2017) and Hua et al. (2013).

The  $\tau_{\text{soc}}$  can be calculated as the inverse of the decomposition rate, that is,  $\tau_{\text{soc}} = 1/k$  (Torn et al., 2009). The numerical optimization of  $k$  was resolved with the function “turnoverfit” by the SoilR package (Sierra et al., 2014). When the bomb-derived radiocarbon yields two possible  $k$ , we identified the right value based on the information on the plant litterfall and the carbon stock (Gaudinski et al., 2000). We used the smaller  $k$  (i.e., longer  $\tau_{\text{soc}}$ ) when litterfall or carbon stock information was missing.

## 2.5. Statistical Analyses

The Shapiro-Wilk normality test (Royston, 1992) was used to test the normality of  $\tau_{\text{soc}}$  and other environmental factors before further analyses. We used the one-way analysis of variance (ANOVA) to examine the statistical significance of  $\tau_{\text{soc}}$  in two soil layers. A  $P$ -value of  $<0.05$  was considered statistically significant. We measured vegetation, climatic, soil chemical, and soil physical properties to analyze the impacts of biotic and abiotic factors on  $\tau_{\text{soc}}$ . The relationship between  $\tau_{\text{soc}}$  and dependent variables was tested by Pearson's correlation and the Partial Mantel test (Mantel, 1967). The Partial Mantel tests were conducted by the function “fortify\_mantel” within the “ggcor” and “vegan” packages in the software R. The statistical analysis to determine the dependent variables of  $\tau_{\text{soc}}$  was performed on the two soil layers (i.e., 0–30 cm, 30–100 cm) separately. The generalized linear model (GLM) was used to identify the relationship between stand age, soil depth, and  $\tau_{\text{soc}}$  (Nelder & Wedderburn, 1972). The importance value of a given predictor is based on the sum of Akaike's weight. All statistical analyses and graphs were performed using the R software (Version 3.5.2, R Development Core Team, 2019). The maps of forest types worldwide and in Eastern China were conducted using ArcGIS software (Version 10.4.1, Environmental System Research Institute, USA, 2016). Structural equation modeling (SEM; Schermelleh-Engel et al., 2003) was used to evaluate the positive and negative relationships between climate, biomass production, SOC stoichiometry, chemical properties, and physical properties on  $\tau_{\text{soc}}$ . The fit of the optimization model was evaluated using the  $Chi$ -square test, and the root means squared error (RMSE). The structural equation modeling analyses were conducted using Amos 21 (Amos Development Corporation, Chicago, USA).

## 3. Results

### 3.1. Spatial Variations of $\tau_{\text{soc}}$

We found that the mean turnover time of bulk soil ( $\tau_{\text{soc}}$ ) in the deep layer ( $>30$  cm) was significantly higher than the surface layer (0–30 cm) both at regional and global scales (Figure 2). Across the 12 permanent forest plots in the Eastern Asian Monsoon region, the mean  $\tau_{\text{soc}}$  of bulk soil was  $249 \pm 80$  years on the surface, which was significantly shorter than the deep layer of  $2,087 \pm 246$  years across the 12 forest plots (Figure 2b,  $P = 0.02$ ). We also observed a large spatial variation of  $\tau_{\text{soc}}$ . Specifically, for the surface layer, the  $\tau_{\text{soc}}$  ranged from 116 years at site BDG to 421 years at site TT with a variation of 54% (Figure 2). The  $\tau_{\text{soc}}$  is characterized by a wide range from 130 years at the site of BDG to 7,508 years at the site CB in the deep layer, with a variance of 133% (Figure S2 in Supporting Information S1). The higher soil  $\Delta^{14}\text{C}$  was observed in the surface layer with a mean value of  $-0.62 \pm 52.89\%$ , while the deeper layer was more depleted with a mean value of  $-191.42 \pm 138.63\%$  (Figure S2 in Supporting Information S1).

On the global scale, the mean  $\tau_{\text{soc}}$  was  $332 \pm 56$  years on the surface and  $3,081 \pm 398$  years in deep layers (Figure 2). Multiple comparisons and analyses of variance (one-way ANOVA with a least significant difference, LSD test) were used to test the vertical distribution of  $\tau_{\text{soc}}$  at the global scale. An increasingly  $\tau_{\text{soc}}$  with soil depth was found at the global scale (Figure 2 and Figure S2 in Supporting Information S1). Positive  $\Delta^{14}\text{C}$  value occurred at the upper 30 cm, representing a SOC pool with the input of atmospheric bomb  $^{14}\text{C}$  (Figure S2 in Supporting Information S1). The deeper layer was characterized by negative values ranging from  $-84.25\%$  at a soil depth of 40 cm to  $-284.43\%$  at a soil depth of 150 cm (Figure S2 in Supporting Information S1). The results of the LSD test demonstrated that the mean  $\tau_{\text{soc}}$  at deep soil layers ( $>30$  cm) was significantly larger than at surface layers (0–30 cm) at both global and regional scales (Figure 2 and Figure S2 in Supporting Information S1).

### 3.2. Biotic and Abiotic Factors Driving the Geographic Relationship

The stand age ranged from 25 to 200 years across the 12 permanent forest plots in the East Asian monsoon region (Figure S1 in Supporting Information S1). The total tree basal area at the breast height ranged from  $17.52 \pm 4.89$  to

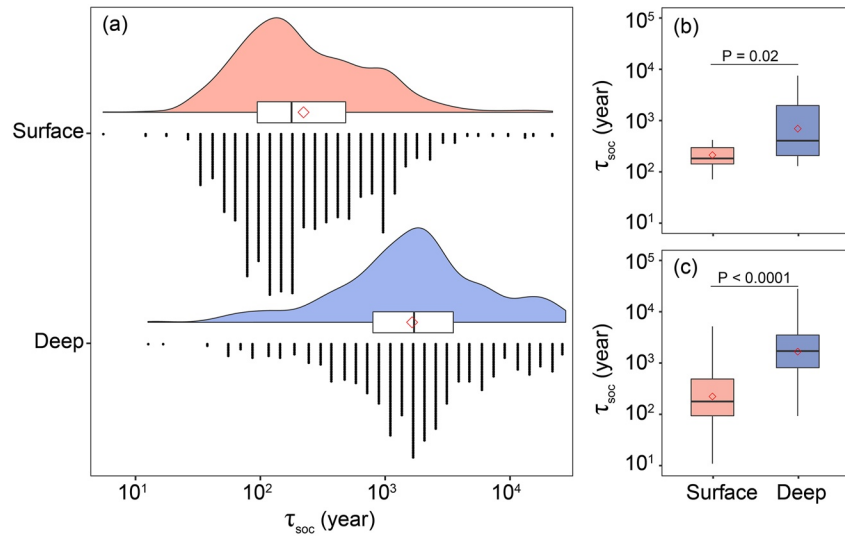


**Figure 2.** Distribution of soil organic carbon (SOC) turnover time ( $\tau_{\text{soc}}$ ) at two soil depths in all data (a,  $n = 1,897$ ), regional analysis (b,  $n = 24$ ), and global synthesis (c,  $n = 1,873$ ). The red and blue shades indicated the density distribution of 1,897 pieces of all data in panel (a). The boxplot indicated the 25th, 50th, and 75th data in all panels. The solid line and diamond shape in the boxplot represented the median and mean values.

$40.18 \pm 9.61 \text{ m}^2 \text{ ha}^{-1}$ , with an increasing trend with stand age (Figure S3a in Supporting Information S1). The mean litter and fine root biomass were  $5.59 \pm 1.93 \text{ Mg ha}^{-1}$  and  $82.61 \pm 76.13 \text{ g cm}^{-2}$ , with no significant trend at the spatial scale ( $P = 0.82$ , Figure S3 and Table S7 in Supporting Information S1). Across the 12 permanent forest plots, the fine root biomass was 1.22-fold in the surface layer than in the deep layer (Figure 3). Soil stoichiometry of the surface layer is 2.57 times for C:P, 1.80 times for N:P, and 1.43 times for C: N in the deep layers (Figure 3 and Table S2 in Supporting Information S1). In contrast, clay content, bulk density, and  $\text{Fe}_2\text{O}_3$  were accumulated in deep layers than the surface layer (Figure 3 and Table S2 in Supporting Information S1). Specifically, the clay content was lower in the surface layer ( $19.99 \pm 4.30\%$ ) than in the deep layer ( $23.56 \pm 6.43\%$ ; Figure S3 in Supporting Information S1).

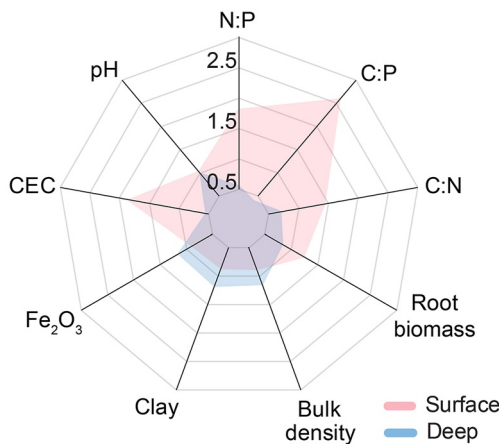


**Figure 3.** The change of soil properties at two soil depths. Radar plots show the change in chemical processes, physical processes, and root biomass at two depths. The chemical processes include CEC (cation exchange capacity in the soil, exchangeable cations per unit weight in dry soil,  $\text{cmol kg}^{-1}$ ), total  $\text{Fe}_2\text{O}_3$  in soil, and pH. The physical processes include clay content and bulk density. Soil properties conclude C:N (the ratio of soil organic carbon [SOC] and total nitrogen content), C:P (the ratio of SOC and total phosphorus content), and N:P (the ratio of total phosphorus and total nitrogen content). It should be noted that the data presented here were the ratio of variables at the surface and deep. For example, the surface soil pH = surface pH/deep pH, and vice versa.

Bulk density in the surface layer ( $1.08 \text{ g/cm}^{-2}$ ) was slightly lower than the deep layer ( $1.26 \text{ g/cm}^{-2}$ , Figure 3 and Figure S3 in Supporting Information S1). The  $\text{Fe}_2\text{O}_3$  in surface layers ( $4.25 \pm 0.80\%$ ) was lower in deep layers ( $4.76 \pm 0.65\%$ ; Figure 3). The CEC in the surface layer was 1.83-fold higher than in the deep layer (Figure 3). pH value slightly varied with soil depth ( $5.53 \pm 0.75$  and  $5.44 \pm 1.00$  for surface and deep layers, respectively; Figure 3).

Results of the Partial Mantel test suggested that CEC ( $R^2 = 0.61$ ,  $P = 0.02$ ) was the significant factor controlling the spatial variation of mean  $\tau_{\text{soc}}$  in the surface soil layer (Figure 4). In the deep soil layer, the variation of  $\tau_{\text{soc}}$  was significantly influenced by  $\text{Fe}_2\text{O}_3$  content ( $R^2 = 0.43$ ,  $P = 0.006$ ) and stand age ( $R^2 = 0.38$ ,  $P = 0.02$ ). A negative relationship existed between SOC and  $\tau_{\text{soc}}$  at the whole soil profiles ( $y = 1841e^{-0.02x}$ ,  $R^2 = 0.25$ ,  $P = 0.01$ ; Figure S4 in Supporting Information S1). However, we did not detect any significant negative relationship between SOC and  $\tau_{\text{soc}}$  when separating the data into two soil increments (Figure S4 and Table S8 in Supporting Information S1). To examine how biotic and abiotic factors regulated the  $\tau_{\text{soc}}$  at two soil depths, we constructed a SEM based on the possible dominant drivers (Figure 5). The SEM explained 36% ( $\chi^2 = 5.72$ ,  $P = 0.17$ ,  $\text{RMSE} = 0.32$ ) and 41% ( $\chi^2 = 0.17$ ,  $P = 0.68$ ,  $\text{RMSE} = 0.00$ ) of the spatial variance in  $\tau_{\text{soc}}$  in the surface and deep layers, respectively (Figure 6). For surface layers, the pH and CEC negatively affected  $\tau_{\text{soc}}$  ( $P = 0.02$ ; Figure 6a). For the deep layers, total  $\text{Fe}_2\text{O}_3$  ( $R^2 = 0.44$ ,  $P < 0.01$ ) and pH ( $R^2 = 0.63$ ,  $P < 0.001$ ) exerted a positive direct effect on  $\tau_{\text{soc}}$  (Figure 5b). Moreover, the vegetation dynamics indirectly affected  $\tau_{\text{soc}}$  by mediating total  $\text{Fe}_2\text{O}_3$  at deep layers ( $R^2 = 0.44$ ,

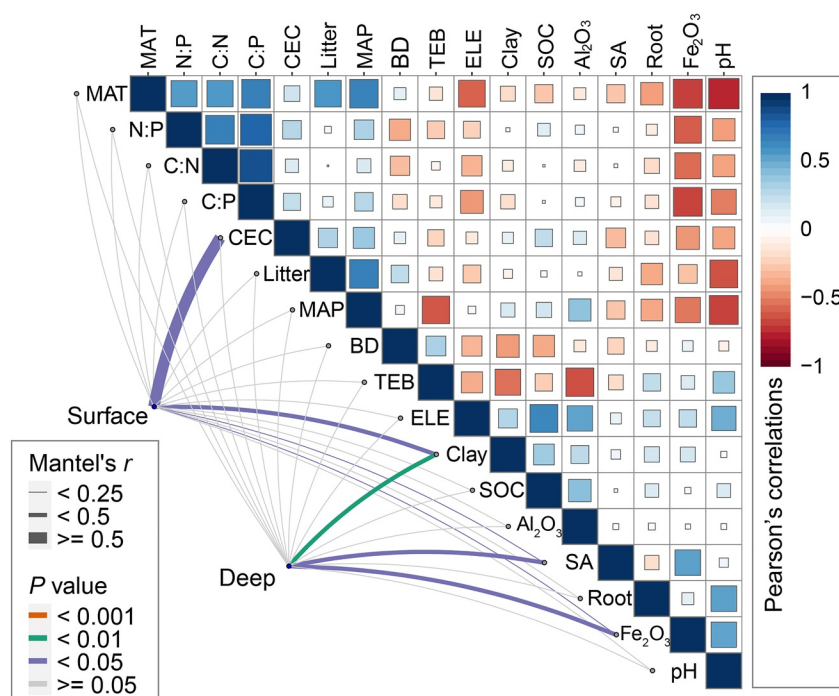


**Figure 4.** Mantel tests and Pearson's correlation matrix illustrate the relationships between site-based  $\tau_{\text{soc}}$  and dependent variables across eastern China. Mantel tests quantified the correlation between  $\tau_{\text{soc}}$  and dependent variables at two soil layers (surface and deep). The line width corresponds to the Partial Mantel's  $r$  statistic for the corresponding correlation, and the line color indicates statistical significance. Color in orange, green, purple, and gray are denoted the significant level of  $<0.001$ ,  $<0.01$ ,  $<0.05$ , and  $>0.05$ , respectively. Pearson's correlation coefficient matrix shows the relationships among dependent variables. Red and blue represent the negative and positive correlations. The significant levels of Pearson's correlation among dependent variables were indicated by square size. The climate drivers conclude the mean annual temperature (MAT) and mean annual precipitation (MAP, mm). The variables of vegetation conclude stand age (SA, year), litter (aboveground accumulated litter biomass,  $\text{Mg ha}^{-1} \text{ year}^{-1}$ ), and root (fine root biomass,  $\text{g cm}^{-2}$ ). The soil properties conclude C:N (the ratio of soil organic carbon [SOC] and total nitrogen content), C:P (the ratio of SOC and total phosphorus content), N:P (the ratio of total phosphorus and total nitrogen content), bulk density (BD,  $\text{g/cm}^3$ ), clay (clay fraction %), cation exchange capacity ([CEC] in the soil, the amount of exchangeable cations per unit weight dry soil,  $\text{cmol kg}^{-1}$ ), total  $\text{Fe}_2\text{O}_3$  (%) and  $\text{Al}_2\text{O}_3$  (%) in soil, pH, and total exchangeable bases (TEB,  $\text{cmol kg}^{-1}$ ). Other property included Ele (Elevation, m).

$P < 0.01$ , Figure 5b). The clay content also showed the influence of spatial variation of  $\tau_{\text{soc}}$ . The climatological factor indirectly affected  $\tau_{\text{soc}}$  by regulating the soil stoichiometric, physical, and chemical properties (Figure 5).

The stand age involved in the global data set ranged from 5 to 400 years with a mean stand age of  $89.65 \pm 77.318$  years, while the soil depth ranged from 0 to 150 cm with a mean value of  $33.65 \pm 32.01$  cm (Figure S6 in Supporting Information S1). All the sampling sites in this study fell into the range of MAT from  $-12.25$  to  $27.70^\circ\text{C}$  and MAP from 88 to 6,910 mm (Figure S7 in Supporting Information S1). By placing the global data of mean  $\tau_{\text{soc}}$  on the Whittaker climate-biome matrix (Whittaker, 1962), we exhibited the combined effect of climatic factors, stand ages, soil depth, and their interactions on  $\tau_{\text{soc}}$  (Figure 6). The results of the multiple regression analysis showed that the fitted model explained 48% of the variability in mean  $\tau_{\text{soc}}$  at the global scale (Figure 6,  $P = 0.03$ ). The climatic and stand age accounted for 1.58% and 1.38% of the variability on global  $\tau_{\text{soc}}$ , respectively. Soil depth accounted for 11.47% of the variance in global  $\tau_{\text{soc}}$  (Figure 6). Interactions between climatic factors, stand age, and soil depth account for 68.62% of the spatial variability in  $\tau_{\text{soc}}$ .

#### 4. Discussion

The mean  $\tau_{\text{soc}}$  is significantly longer in the soil layer below 30 cm than in the topsoil at the regional and global scale, consistent with recent reports (Mathieu et al., 2015; Shi et al., 2020). The geographic variation of  $\tau_{\text{soc}}$  is regulated by the interactive effects of climate, vegetation, and soil properties, with a different mechanism at two soil layers.



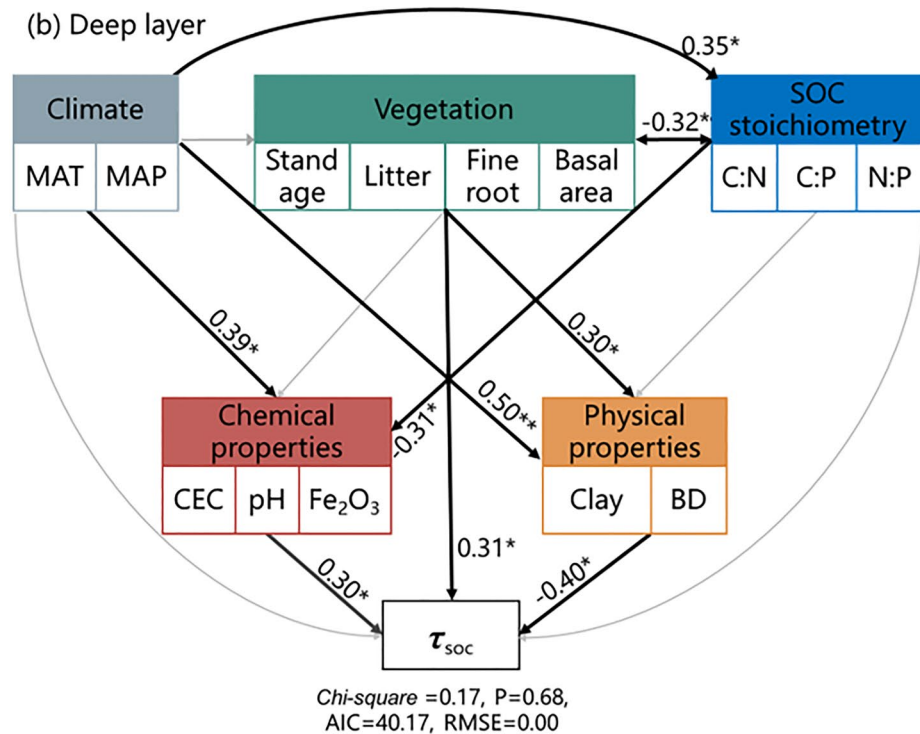
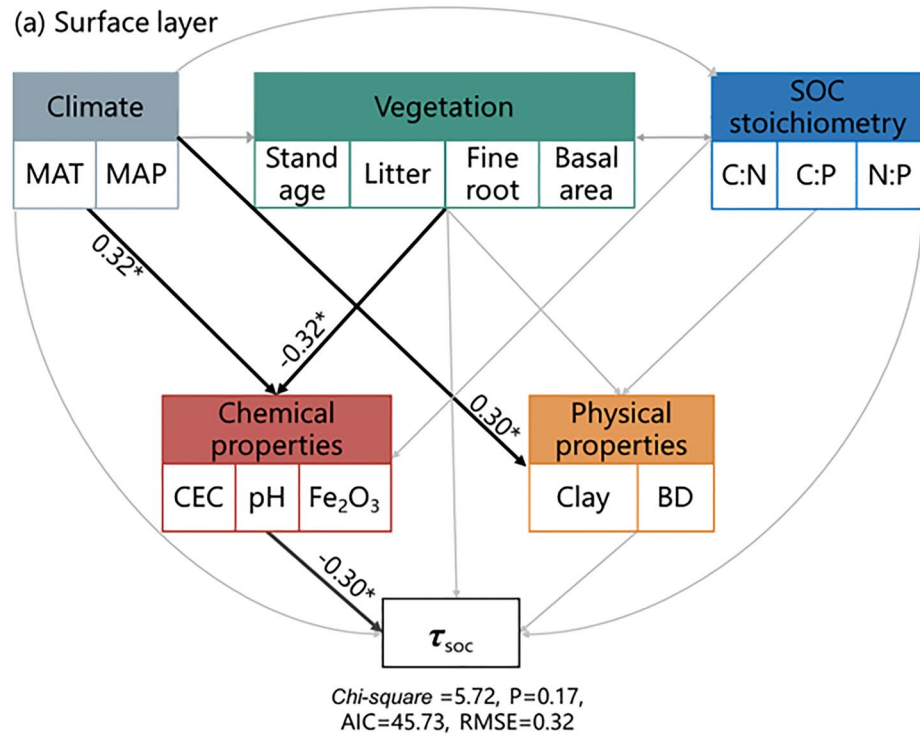


**Figure 5.** Direct and indirect effects of biotic and abiotic variables on the soil organic carbon (SOC) turnover times ( $\tau_{SOC}$ ) at two soil depths. Black solid arrows indicate significant relationships, respectively. Gray dash arrows indicate an insignificant relationship. Numbers at solid arrows ( $P < 0.05$ ) were standardized path coefficients, and the width of the arrows indicated the strength of the relationships. The gray arrows indicated nonsignificant relationships ( $P > 0.05$ ). Numbers close to variables ( $R^2$ ) indicated the variance explained by the pathway analysis.

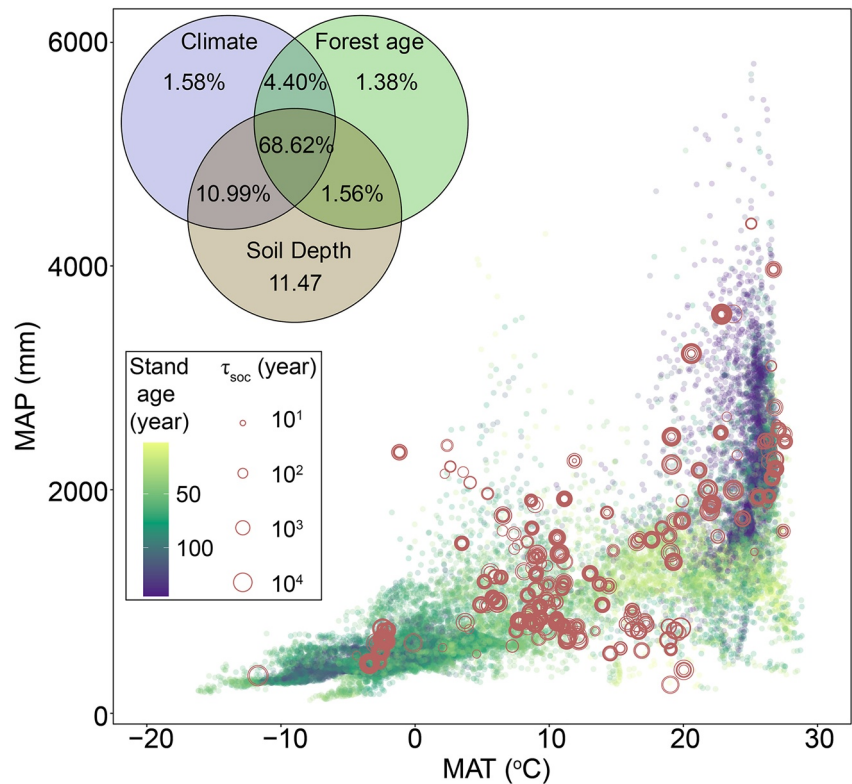


**Figure 6.** Distribution of soil organic carbon (SOC) turnover time ( $\tau_{\text{soc}}$ ) and forest aging under different climate zones ( $N = 1,897$ ). The solid point with different color bars represents the stand age at forest regional under  $1^\circ \times 1^\circ$  grid cells. The empty red point indicates the value  $\tau_{\text{soc}}$ . The relative contribution of stand age, soil depth, and climatic variables on  $\tau_{\text{soc}}$  was tested by the general linear regression model.

Cation-exchange capacity measures soil fertility and represents the maximum of the total exchangeable cations in the soil at a given pH value. A negative relationship between CEC and  $\tau_{\text{soc}}$  has been reported for multiple potential reasons (Solly et al., 2020; Z. Yu et al., 2020). Some site studies have provided evidence that the changes in forest development affected the CEC (Gruba & Mulder, 2015) and further manipulated  $\tau_{\text{soc}}$  (Lawrence et al., 2015). Caused by the high rates of soil weathering and acidification (Jiang et al., 2018), a lower value of CEC can be found in older forests in previous studies (Gilliam et al., 1995; Pincus et al., 2017). This study found a decrease in cation exchange capacity and pH decreases with stand age, resulting in a longer  $\tau_{\text{soc}}$  in the surface soil layer (Figure 5; Figure S5 in Supporting Information S1). The hydrolysis by weathering removes labile, rapidly cycling carbon, leaving behind slower cycling carbon in soil (Clift et al., 2014; Jiang et al., 2018; Solly et al., 2020; Trumbore & Zheng, 1996). With a higher level of CEC in rich SOC conditions, the negative relationship between SOC and  $\tau_{\text{soc}}$  in our study further supported this underlying mechanism (Figure S4b in Supporting Information S1; Lawrence et al., 2015; Paul et al., 2001). Furthermore, reducing soil nutrient availability with forest aging indirectly can enhance the carbon persistence in the forest ecosystem (Posada & Schuur, 2011; Van der Voort et al., 2016). The decrease in CEC would impede the substitution of ammonium in the topsoil (Sollins et al., 1988), reducing N:P ratios in the surface layers associated with forest aging (Figure S3f in Supporting Information S1). A lower mean value of N:P in the older forest than in the younger forest (Figure S3 in Supporting Information S1) is likely due to the higher reduction in soil phosphorus content than nitrogen content. Previous studies have shown that physical protection by clay is one of the active processes that persist in soil organic carbon (Torn et al., 2009; Van der Voort et al., 2019). This study found a negative relationship between clay fraction and  $\tau_{\text{soc}}$  (Figure S5 in Supporting Information S1). Although the correlation between clay content and  $\tau_{\text{soc}}$  was observed, a small spatial variation of clay content in our study may not be sufficient to explain the effects on surface  $\tau_{\text{soc}}$ , especially under forest aging. These results highlight that soil geochemical processes with stand age change could be more important than physical protection in driving the surface soil  $\tau_{\text{soc}}$  variation in the East Asian monsoon region.

A different interaction between soil factors and vegetation on  $\tau_{\text{soc}}$  variation has been found in the deep layers (Figure 5). Mineral protection consisting of total  $\text{Fe}_2\text{O}_3$  content interacting with soil organic carbon to form stable organic minerals is the critical mechanism for carbon persistence in the long term (Kleber et al., 2005). Our results showed that total  $\text{Fe}_2\text{O}_3$  content and its covariance with pH and stand age are the main factors regulating  $\tau_{\text{soc}}$  at deep layers (Figure S5 in Supporting Information S1). The mineral particles with total  $\text{Fe}_2\text{O}_3$  can protect the soil organic matter from microbial decomposition in acidic soils (Colombo et al., 2014). Soil acidification along forest aging gradients, indicated by the decreased pH, further leads to more accumulation of total  $\text{Fe}_2\text{O}_3$  content and slow carbon cycling rates (Figure S3 in Supporting Information S1). Soil total  $\text{Fe}_2\text{O}_3$  is often used as one of the most stable and objective indicators to describe soil development and classification (Hong et al., 2010; M. Yu et al., 2019). Notably, the total  $\text{Fe}_2\text{O}_3$  content measured in this study includes iron from secondary mineral phases (Fe oxyhydroxides) and primary minerals that have not undergone weathering. Thus, some portion of the Fe is locked in the primary mineral structures and not interacting with organic matter. Additionally, the stoichiometry of soil carbon, nitrogen, and phosphorus also affected  $\tau_{\text{soc}}$  through a combined effect of stand age and climate in the deep layer (Figure 5). These findings emphasize that mineral protection could be a critical mechanism to explain the positive correlation between forest stand age and subsoil  $\tau_{\text{soc}}$  in the East Asian monsoon region.

Although paleoclimate evidence has revealed a negative role of climate change in  $\tau_{\text{soc}}$  in the low-latitude monsoon forests (Hein et al., 2020), our study did not find a significant correlation between  $\tau_{\text{soc}}$  and mean annual temperature or mean annual precipitation at the regional and global scales (Figure S7 in Supporting Information S1). However, significant correlations were detected between the climatic factors and total  $\text{Fe}_2\text{O}_3$  content, soil pH, and soil stoichiometry (Figure 4, Pearson's correlation matrix) at the regional scale. It indicated the indirect effects of climatic factors on  $\tau_{\text{soc}}$  by changing soil chemical properties, particularly significant in the deep layer (Figure 5). Consistent with regional results, the variation partitions analysis showed that climatic factors account for a few proportions of the variance in global  $\tau_{\text{soc}}$  (1.58%). In contrast, its interaction with stand age and soil depth can account for 68.62%. These results imply (Figure 6). These results imply the co-influence of climate, stand age, and soil depth on the spatial variation of  $\tau_{\text{soc}}$  (Figure 6). This study examined the available factors widely proposed in previous studies, such as climatic factors (He et al., 2016; Shi et al., 2020) or soil properties (Heckman et al., 2022). Meanwhile, we encounter a prevalent challenge of the weak correlation between  $\tau_{\text{soc}}$  derived from radiocarbon and other factors at the regional and global scale (Herold et al., 2014; Khomo et al., 2017). This weak correlation is possibly due to the high heterogeneity of SOC and variability of  $\tau_{\text{soc}}$  (Van der Voort et al., 2016), indicating complicated interactive effects of physiochemical processes in regulating  $\tau_{\text{soc}}$ . Therefore, acquiring high-precision data along the soil vertical profiles based on the specific sites is essential to improve the explanatory potential of carbon sequestration. Furthermore, more well-designed network experiments and site-specific times characteristic of carbon in plant organs and soil layers help upscale the site-specific research into global projection. Adding the vertical soil processes and their interactions with climate and vegetation factors is needed to improve the projections of the forest carbon cycle in the Earth system models (He et al., 2016; Koven et al., 2013; J. Wang et al., 2019; Wei et al., 2022).

## 5. Conclusion

By sampling soils from 12 forest plots, this study further detected a higher complexity of interaction between biotic and abiotic factors in driving the spatial variation of  $\tau_{\text{soc}}$  in the deep than surface soil layer. Based on an extensive data set, this study revealed a joint regulation of climate, vegetation, and soil factors on the spatial variation of soil carbon persistence on a global scale. Mineral protection by iron oxide is critical in explaining the positive correlation between forest stand age and deep soil carbon persistence. These findings call for more efforts on the mechanisms underlying the interactions of climate, vegetation, and soil factors in driving soil carbon persistence in global forests. This study also recommends more measurements of the carbon ages in different plant organs and soil layers on the ecosystem level. The global patterns of  $\tau_{\text{soc}}$  at different soil depths are useful to inform Earth system models, which incorporate forest vegetation dynamics and multiple soil layers and their interactions.

## Conflict of Interest

The authors declare no conflicts of interest relevant to this study.

## Data Availability Statement

The data that support the findings of this study are publicly available on the Zenodo data repository (<https://doi.org/10.5281/zenodo.7623837>).

### Acknowledgments

We thank Dr. Fangliang He for providing information and assistance with the Heishiding plot. This work was financially supported by the National Natural Science Foundation of China (31800400, 42201062).

### References

- Anderson-Teixeira, K. J., Wang, M. M., McGarvey, J. C., Herrmann, V., Tepley, A. J., Bond-Lamberty, B., & LeBauer, D. S. (2018). ForC: A global database of forest carbon stocks and fluxes. *Ecology*, 99(6), 1507. <https://doi.org/10.1002/ecy.2229>
- Angst, G., Mueller, K. E., Eissenstat, D. M., Trumbore, S., Freeman, K. H., Hobbie, S. E., et al. (2019). Soil organic carbon stability in forests: Distinct effects of tree species identity and traits. *Global Change Biology*, 25(4), 1529–1546. <https://doi.org/10.1111/gcb.14548>
- Besnard, S., Carvalhais, N., Arain, M. A., Black, A., De Bruin, S., Buchmann, N., et al. (2018). Quantifying the effect of forest age in annual net forest carbon balance. *Environmental Research Letters*, 13(12), 124018. <https://doi.org/10.1088/1748-9326/aaeaeab>
- Bonan, G. B. (2016). Forests, climate, and public policy: A 500-year interdisciplinary odyssey. *Annual Review of Ecology, Evolution, and Systematics*, 47(1), 97–121. <https://doi.org/10.1146/annurev-ecolsys-121415-032359>
- Børja, I., De Wit, H. A., Steffenrem, A., & Majdi, H. (2008). Stand age and fine root biomass, distribution and morphology in a Norway spruce chronosequence in southeast Norway. *Tree Physiology*, 28(5), 773–784. <https://doi.org/10.1093/treephys/28.5.773>
- Carmona, C. P., Bueno, C. G., Toussaint, A., Träger, S., Díaz, S., Moora, M., et al. (2021). Fine-root traits in the global spectrum of plant form and function. *Nature*, 597(7878), 683–687. <https://doi.org/10.1038/s41586-021-03871-y>
- Carvalhais, N., Forkel, M., Khomik, M., Bellarby, J., Jung, M., Migliavacca, M., et al. (2014). Global covariation of carbon turnover times with climate in terrestrial ecosystems. *Nature*, 514(7521), 213–217. <https://doi.org/10.1038/nature13731>
- Chen, C., Hall, S. J., Coward, E., & Thompson, A. (2020). Iron-mediated organic matter decomposition in humid soils can counteract protection. *Nature Communications*, 11(1), 2255. <https://doi.org/10.1038/s41467-020-16071-5>
- Chen, L., Fang, K., Wei, B., Qin, S., Feng, X., Hu, T., et al. (2021). Soil carbon persistence governed by plant input and mineral protection at regional and global scales. *Ecology Letters*, 24(5), 1018–1028. <https://doi.org/10.1111/ele.13723>
- Chen, X., Taylor, A. R., Reich, P. B., Hisano, M., Chen, H. Y., & Chang, S. X. (2023). Tree diversity increases decadal forest soil carbon and nitrogen accrual. *Nature*, 618(7963), 94–101. <https://doi.org/10.1038/s41586-023-05941-9>
- Clift, P. D., Wan, S., & Blusztajn, J. (2014). Reconstructing chemical weathering, physical erosion and monsoon intensity since 25Ma in the northern South China Sea: A review of competing proxies. *Earth-Science Reviews*, 130, 86–102. <https://doi.org/10.1016/j.earscirev.2014.01.002>
- Colombo, C., Palumbo, G., He, J. Z., Pinton, R., & Cesco, S. (2014). Review on iron availability in soil: Interaction of Fe minerals, plants, and microbes. *Journal of Soils and Sediments*, 14(3), 538–548. <https://doi.org/10.1007/s11368-013-0814-z>
- Curtis, P. S., & Gough, C. M. (2018). Forest aging, disturbance and the carbon cycle. *New Phytologist*, 219(4), 1188–1193. <https://doi.org/10.1111/nph.15227>
- Dai, Y., Shangguan, W., Wei, N., Xin, Q., Yuan, H., Zhang, S., et al. (2019). A review of the global soil property maps for Earth system models. *Soil*, 5(2), 137–158. <https://doi.org/10.5194/soil-5-137-2019>
- Doetterl, S., Berhe, A. A., Arnold, C., Bodé, S., Fiener, P., Finke, P., et al. (2018). Links among warming, carbon and microbial dynamics mediated by soil mineral weathering. *Nature Geoscience*, 11(8), 589–593. <https://doi.org/10.1038/s41561-018-0168-7>
- Doetterl, S., Stevens, A., Six, J., Merckx, R., Van Oost, K., Casanova Pinto, M., et al. (2015). Soil carbon storage controlled by interactions between geochemistry and climate. *Nature Geoscience*, 8(10), 780–783. <https://doi.org/10.1038/ngeo2516>
- Fontaine, S., Barot, S., Barré, P., Bdioui, N., Mary, B., & Rumpel, C. (2007). Stability of organic carbon in deep soil layers controlled by fresh carbon supply. *Nature*, 450(7167), 277–280. <https://doi.org/10.1038/nature06275>
- Friedl, M., & Sulla-Menashe, D. (2022). MODIS/Terra+Aqua land cover type yearly L3 global 500m SIN grid V061. NASA EOSDIS Land Processes DAAC. <https://doi.org/10.5067/MODIS/MCD12Q1.061>
- Friedlingstein, P., Jones, M. W., O'Sullivan, M., Andrew, R. M., Bakker, D. C., Hauck, J., et al. (2022). Global carbon budget 2021. *Earth System Science Data*, 14(4), 1917–2005. <https://doi.org/10.5194/essd-14-1917-2022>
- Gaudinski, J. B., Trumbore, S. E., Davidson, E. A., & Zheng, S. (2000). Soil carbon cycling in a temperate forest: Radiocarbon-based estimates of residence times, sequestration rates and partitioning of fluxes. *Biogeochemistry*, 51(1), 33–69. <https://doi.org/10.1023/A:1006301010014>
- Ge, R., He, H., Zhang, L., Ren, X., Williams, M., Yu, G., et al. (2022). Climate sensitivities of carbon turnover times in soil and vegetation: Understanding their effects on forest carbon sequestration. *Journal of Geophysical Research: Biogeosciences*, 127(3), e2020JG005880. <https://doi.org/10.1029/2020JG005880>
- Germon, A., Laclau, J.-P., Robin, A., & Jourdan, C. (2020). Tamm review: Deep fine roots in forest ecosystems: Why dig deeper? *Forest Ecology and Management*, 466, 118135. <https://doi.org/10.1016/j.foreco.2020.118135>
- Gilliam, F. S., Turrill, N. L., & Adams, M. B. (1995). Herbaceous-layer and overstory species in clear-cut and mature central Appalachian hardwood forests. *Ecological Applications*, 5(4), 947–955. <https://doi.org/10.2307/2269345>
- Gruba, P., & Mulder, J. (2015). Tree species affect cation exchange capacity (CEC) and cation binding properties of organic matter in acid forest soils. *Science of the Total Environment*, 511, 655–662. <https://doi.org/10.1016/j.scitotenv.2015.01.013>
- Hammer, S., & Levin, I. (2017). Monthly mean atmospheric  $\Delta^{14}\text{C}_{\text{CO}_2}$  at Jungfraujoch and Schauinsland from 1986 to 2016 [Dataset]. <https://doi.org/10.11588/data/10100>
- He, Y., Trumbore, S. E., Torn, M. S., Harden, J. W., Vaughn, L. J., Allison, S. D., & Randerson, J. T. (2016). Radiocarbon constraints imply reduced carbon uptake by soils during the 21st century. *Science*, 353(6306), 1419–1424. <https://doi.org/10.1126/science.aad4273>
- Heckman, K., Pries, C. E. H., Lawrence, C. R., Rasmussen, C., Crow, S. E., Hoyt, A. M., et al. (2022). Beyond bulk: Density fractions explain heterogeneity in global soil carbon abundance and persistence. *Global Change Biology*, 28(3), 1178–1196. <https://doi.org/10.1111/gcb.16023>
- Hein, C. J., Usman, M., Eglinton, T. I., Haghypour, N., & Galy, V. V. (2020). Millennial-scale hydroclimate control of tropical soil carbon storage. *Nature*, 581(7806), 63–66. <https://doi.org/10.1038/s41586-020-2233-9>
- Herold, N., Schöning, I., Michalzik, B., Trumbore, S., & Schruppf, M. (2014). Controls on soil carbon storage and turnover in German landscapes. *Biogeochemistry*, 119(1–3), 435–451. <https://doi.org/10.1007/s10533-014-9978-x>
- Holdaway, R. J., Richardson, S. J., Dickie, I. A., Peltzer, D. A., & Coomes, D. A. (2011). Species- and community-level patterns in fine root traits along a 120000-year soil chronosequence in temperate rain forest. *Journal of Ecology*, 99(4), 954–963. <https://doi.org/10.1111/j.1365-2745.2011.01821.x>
- Hong, H., Gu, Y., Li, R., Zhang, K., & Li, Z. (2010). Clay mineralogy and geochemistry and their palaeoclimatic interpretation of the Pleistocene deposits in the Xuancheng section, southern China. *Journal of Quaternary Science*, 25(5), 662–674. <https://doi.org/10.1002/jqs.1340>
- Hua, Q., Barbetti, M., & Rakowski, A. Z. (2013). Atmospheric radiocarbon for the period 1950–2010. *Radiocarbon*, 55(4), 2059–2072. [https://doi.org/10.2458/azu\\_js\\_rc.v55i2.16177](https://doi.org/10.2458/azu_js_rc.v55i2.16177)
- Jiang, J., Wang, Y. P., Yu, M., Cao, N., & Yan, J. (2018). Soil organic matter is important for acid buffering and reducing aluminum leaching from acidic forest soils. *Chemical Geology*, 501, 86–94. <https://doi.org/10.1016/j.chemgeo.2018.10.009>
- Kaiser, K., & Guggenberger, G. (2003). Mineral surfaces and soil organic matter. *European Journal of Soil Science*, 54(2), 219–236. <https://doi.org/10.1046/j.1365-2389.2003.00544.x>

- Keeney, A., & Page, A. L. (1982). *Methods of soil analysis*. American Society of Agronomy, Inc. 1986.
- Khomo, L., Trumbore, S., Bern, C. R., & Chadwick, O. A. (2017). Timescales of carbon turnover in soils with mixed crystalline mineralogies. *Soil*, 3(1), 17–30. <https://doi.org/10.5194/soil-3-17-2017>
- Kleber, M., Mikutta, R., Torn, M. S., & Jahn, R. (2005). Poorly crystalline mineral phases protect organic matter in acid subsoil horizons. *European Journal of Soil Science*, 56(0), 717–725. <https://doi.org/10.1111/j.1365-2389.2005.00706.x>
- Koven, C. D., Riley, W. J., Subin, Z. M., Tang, J. Y., Torn, M. S., Collins, W. D., et al. (2013). The effect of vertically resolved soil biogeochemistry and alternate soil C and N models on C dynamics of CLM4. *Biogeosciences*, 10(11), 7109–7131. <https://doi.org/10.5194/bg-10-7109-2013>
- Lawrence, C. R., Beem-Miller, J., Hoyt, A. M., Monroe, G., Sierra, C. A., Stoner, S., et al. (2020). An open-source database for the synthesis of soil radiocarbon data: International Soil Radiocarbon Database (ISRAD) version 1.0. *Earth System Science Data*, 12(1), 61–76. <https://doi.org/10.5194/essd-12-61-2020>
- Lawrence, C. R., Harden, J. W., Xu, X., Schulz, M., & Trumbore, S. (2015). Long-term controls on soil organic carbon with depth and time: A case study from the Cowlitz River chronosequence, WA USA. *Geoderma*, 247, 73–87. <https://doi.org/10.1016/j.geoderma.2015.02.005>
- Liu, G. S., Jiang, N. H., Zhang, L. D., & Liu, Z. L. (1996). Soil physical and chemical analysis and description of soil profiles. *China Standard Methods Press, Beijing, China*, 24, 266.
- Luo, Z., Wang, G., & Wang, E. (2019). Global subsoil organic carbon turnover times dominantly controlled by soil properties rather than climate. *Nature Communications*, 10(1), 3688. <https://doi.org/10.1038/s41467-019-11597-9>
- Lützow, M. V., Kögel-Knabner, I., Ekschmitt, K., Matzner, E., Guggenberger, G., Marschner, B., & Flessa, H. (2006). Stabilization of organic matter in temperate soils: Mechanisms and their relevance under different soil conditions – A review. *European Journal of Soil Science*, 57(4), 426–445. <https://doi.org/10.1111/j.1365-2389.2006.00809.x>
- Mantel, N. (1967). The detection of disease clustering and a generalized regression approach. *Cancer Research*, 27, 209–220.
- Mathieu, J. A., Hatté, C., Balesdent, J., & Parent, E. (2015). Deep soil carbon dynamics are driven more by soil type than by climate: A worldwide meta-analysis of radiocarbon profiles. *Global Change Biology*, 21(11), 4278–4292. <https://doi.org/10.1111/gcb.13012>
- McDowell, N. G., Allen, C. D., Anderson-Teixeira, K., Aukema, B. H., Bond-Lamberty, B., Chini, L., et al. (2020). Pervasive shifts in forest dynamics in a changing world. *Science*, 368(6494), eaaz946. <https://doi.org/10.1126/science.aaz9463>
- Müller, T., & Höper, H. (2004). Soil organic matter turnover as a function of the soil clay content: Consequences for model applications. *Soil Biology and Biochemistry*, 36(6), 877–888. <https://doi.org/10.1016/j.soilbio.2003.12.015>
- Murphy, J., & Riley, J. P. (1962). A modified single solution method for the determination of phosphate in natural waters. *Analytica Chimica Acta*, 27, 31–36. [https://doi.org/10.1016/s0003-2670\(00\)88444-5](https://doi.org/10.1016/s0003-2670(00)88444-5)
- Nabel, J. E. M. S., Naudts, K., & Pongratz, J. (2020). Accounting for forest age in the tile-based dynamic global vegetation model JSBACH4 (4.20p7; git feature/forests) – A land surface model for the ICON-ESM. *Geoscientific Model Development*, 13(1), 185–200. <https://doi.org/10.5194/gmd-13-185-2020>
- Nelder, J. A., & Wedderburn, R. W. (1972). Generalized linear models. *Journal of the Royal Statistical Society: Series A (General)*, 135(3), 370–384. <https://doi.org/10.2307/2344614>
- Paul, E. A., Collins, H. P., & Leavitt, S. W. (2001). Dynamics of resistant soil carbon of Midwestern agricultural soils measured by naturally occurring <sup>14</sup>C abundance. *Geoderma*, 104(3–4), 239–256. [https://doi.org/10.1016/S0016-7061\(01\)00083-0](https://doi.org/10.1016/S0016-7061(01)00083-0)
- Pincus, L. N., Ryan, P. C., Huertas, F. J., & Alvarado, G. E. (2017). The influence of soil age and regional climate on clay mineralogy and cation exchange capacity of moist tropical soils: A case study from Late Quaternary chronosequences in Costa Rica. *Geoderma*, 308, 130–148. <https://doi.org/10.1016/j.geoderma.2017.08.033>
- Posada, J. M., & Schuur, E. A. (2011). Relationships among precipitation regime, nutrient availability, and carbon turnover in tropical rain forests. *Oecologia*, 165(3), 783–795. <https://doi.org/10.1007/s00442-010-1881-0>
- Poulter, B., Aragão, L., Andela, N., Bellassen, V., Ciais, P., Kato, T., et al. (2019). The global forest age dataset (GFADv1.1). *NASA National Aeronautics and Space Administration*. <https://doi.org/10.1594/PANGAEA.897392>
- Qiao, Y., Wang, J., Liu, H., Huang, K., Yang, Q., Lu, R., et al. (2020). Depth-dependent soil C-N-P stoichiometry in a mature subtropical broadleaf forest. *Geoderma*, 370, 114357. <https://doi.org/10.1016/j.geoderma.2020.114357>
- Quideau, S. A., Chadwick, O. A., Benesi, A., Graham, R. C., & Anderson, M. A. (2001). A direct link between forest vegetation type and soil organic matter composition. *Geoderma*, 104(1–2), 41–60. [https://doi.org/10.1016/S0016-7061\(01\)00055-6](https://doi.org/10.1016/S0016-7061(01)00055-6)
- Royston, P. (1992). Approximating the Shapiro-Wilk W-test for non-normality. *Statistics and Computing*, 2(3), 117–119. <https://doi.org/10.1007/bf01891203>
- Schermelleh-Engel, K., Moosbrugger, H., & Müller, H. (2003). Evaluating the fit of structural equation models: Tests of significance and descriptive goodness-of-fit measures. *Methods of Psychological Research Online*, 8, 23–74. Retrieved from <http://www.mpr-online.de>
- Schmidt, M. W., Torn, M. S., Abiven, S., Dittmar, T., Guggenberger, G., Janssens, I. A., et al. (2011). Persistence of soil organic matter as an ecosystem property. *Nature*, 478(7367), 49–56. <https://doi.org/10.1038/nature10386>
- Schuur, E. A., Druffel, E. R., & Trumbore, S. E. (2016). *Radiocarbon and climate change*. Springer.
- Shi, Z., Allison, S. D., He, Y., Levine, P. A., Hoyt, A. M., Beem-Miller, J., et al. (2020). The age distribution of global soil carbon inferred from radiocarbon measurements. *Nature Geoscience*, 13(8), 555–559. <https://doi.org/10.1038/s41561-020-0596-z>
- Sierra, C. A., Muller, M., Metzler, H., Manzoni, S., & Trumbore, S. E. (2016). The muddle of ages, turnover, transit, and residence times in the carbon cycle. *Global Change Biology*, 23(5), 1763–1773. <https://doi.org/10.1111/gcb.13556>
- Sierra, C. A., Müller, M., & Trumbore, S. E. (2014). Modeling radiocarbon dynamics in soils: SoilR version 1.1. *Geoscientific Model Development*, 7(5), 1919–1931. <https://doi.org/10.5194/gmd-7-1919-2014>
- Sollins, P., Robertson, G. P., & Uehara, G. (1988). Nutrient mobility in variable- and permanent-charge soils. *Biogeochemistry*, 6(3), 181–199. <https://doi.org/10.1007/BF02182995>
- Solly, E. F., Weber, V., Zimmermann, S., Walthert, L., Hagedorn, F., & Schmidt, M. W. (2020). A critical evaluation of the relationship between the effective cation exchange capacity and soil organic carbon content in Swiss forest soils. *Frontiers in Forests and Global Change*, 3, 98. <https://doi.org/10.3929/ethz-b-000457241>
- Stuiver, M., & Polach, H. A. (1977). Discussion reporting of <sup>14</sup>C data. *Radiocarbon*, 19(3), 355–363. <https://doi.org/10.1017/S0033822200003672>
- Tardif, D., Fluteau, F., Donnadieu, Y., Hir, G. L., Ladant, J. B., Sepulchre, P., et al. (2020). The origin of Asian monsoons: A modelling perspective. *Climate of the Past*, 16(3), 847–865. <https://doi.org/10.5194/cp-16-847-2020>
- Tian, H., Melillo, J. M., Kicklighter, D. W., Pan, S., Liu, J., McGuire, A. D., & Moore, B., III. (2003). Regional carbon dynamics in monsoon Asia and its implications for the global carbon cycle. *Global and Planetary Change*, 37, 201–217. [https://doi.org/10.1016/S0921-8181\(02\)00205-9](https://doi.org/10.1016/S0921-8181(02)00205-9)
- Torn, M. S., Swanston, C. W., Castanha, C., & Trumbore, S. E. (2009). Storage and turnover of organic matter in soil. In *Biophysico chemical processes involving natural nonliving organic matter in environmental systems*. Wiley.

- Torn, M. S., Trumbore, S. E., Chadwick, O. A., Vitousek, P. M., & Hendricks, D. M. (1997). Mineral control of soil organic carbon storage and turnover. *Nature*, 389(6647), 170–173. <https://doi.org/10.1038/38260>
- Trumbore, S. E. (1997). Potential responses of soil organic carbon to global environmental change. *Proceedings of the National Academy of Sciences*, 94(16), 8284–8291. <https://doi.org/10.1073/pnas.94.16.828>
- Trumbore, S. E. (2009). Radiocarbon, and soil carbon dynamics. *Annual Review of Earth and Planetary Sciences*, 37(1), 47–66. <https://doi.org/10.1146/annurev.earth.36.031207.124300>
- Trumbore, S. E., & Zheng, S. (1996). Comparison of fractionation methods for soil organic matter  $^{14}\text{C}$  analysis. *Radiocarbon*, 38(2), 219–229. <https://doi.org/10.1017/S003822200017598>
- USDA. (1996). *Natural Resources Conservation Services, Nation Soil Survey Center, 1996 USDA, Natural Resources Conservation Services, Nation Soil Survey Center Soil Survey Laboratory Manual* (Soil Survey Investigation Report No. 1). U.S. Dept. Agric.
- Van der Voort, T. S., Hagedorn, F., McIntyre, C., Zell, C., Walthert, L., Schleppli, P., et al. (2016). Variability in  $^{14}\text{C}$  contents of soil organic matter at the plot and regional scale across climatic and geologic gradients. *Biogeosciences*, 13(11), 3427–3439. <https://doi.org/10.5194/bg-13-3427-2016>
- Van der Voort, T. S., Mannu, U., Hagedorn, F., McIntyre, C., Walthert, L., Schleppli, P., et al. (2019). Dynamics of deep soil carbon—insights from  $^{14}\text{C}$  time series across a climatic gradient. *Biogeosciences*, 16, 3233–3246. <https://doi.org/10.5194/bg-16-3233-2019>
- Wang, J., Xia, J., Zhou, X., Huang, K., Zhou, J., Huang, Y., et al. (2019). Evaluating the simulated mean soil carbon transit times by Earth system models using observations. *Biogeosciences*, 16(4), 917–926. <https://doi.org/10.5194/bg-16-917-2019>
- Wang, M., Guo, X., Zhang, S., Xiao, L., Mishra, U., Yang, Y., et al. (2022). Global soil profiles indicate depth-dependent soil carbon losses under a warmer climate. *Nature Communication*, 13(1), 5514. <https://doi.org/10.1038/s41467-022-33278-w>
- Wei, N., Xia, J., Zhou, J., Jiang, L., Cui, E., Ping, J., & Luo, Y. (2022). Evolution of uncertainty in terrestrial carbon storage in earth system models from CMIP5 to CMIP6. *Journal of Climate*, 35(17), 1–33. <https://doi.org/10.1175/JCLI-D-21-0763.1>
- Whittaker, R. H. (1962). Classification of natural communities. *The Botanical Review*, 28, 1–239. <https://doi.org/10.1007/bf02860872>
- Yu, M., Wang, Y., Jiang, J., Wang, C., Zhou, G., & Yan, J. (2019). Soil organic carbon stabilization in the three subtropical forests: Importance of clay and metal oxides. *Journal of Geophysical Research: Biogeosciences*, 124(10), 2976–2990. <https://doi.org/10.1029/2018JG004995>
- Yu, Z., Chen, H. Y., Searle, E. B., Sardans, J., Ciais, P., Peñuelas, J., & Huang, Z. (2020). Whole soil acidification and base cation reduction across subtropical China. *Geoderma*, 361, 114107. <https://doi.org/10.1016/j.geoderma.2019.114107>
- Zhu, C., & Xia, J. (2020). Nonlinear increase of vegetation carbon storage in aging forests and its implication for Earth system models. *Journal of Advances in Modeling Earth Systems*, 12, e2020MS002304. <https://doi.org/10.1029/2020MS002304>

## References From the Supporting Information

- Anderson-Teixeira, K. J., Davies, S. J., Bennett, A. C., Gonzalez-Akre, E. B., Muller-Landau, H. C., Joseph Wright, S., et al. (2015). CTFS-forest GEO: A worldwide network monitoring forests in an era of global change. *Global Change Biology*, 21(2), 528–549. <https://doi.org/10.1111/gcb.12712>
- Bruehlheide, H., Böhnke, M., Both, S., Fang, T., Assmann, T., Baruffol, M., et al. (2011). Community assembly during secondary forest succession in a Chinese subtropical forest. *Ecological Monographs*, 81(1), 25–41. <https://doi.org/10.1890/09-2172.1>
- Chu, C., Lutz, J. A., Král, K., Vrška, T., Yin, X., Myers, J. A., & He, F. (2019). Direct and indirect effects of climate on richness drive the latitudinal diversity gradient in forest trees. *Ecology Letters*, 22, 245–255. <https://doi.org/10.1111/ele.13175>
- Condit, R. (1998). *Tropical forest census plots: Methods and results from Barro Colorado Island, Panama and a comparison with other plots*. Springer Science & Business Media.
- Fu, B. J., Liu, S. L., Ma, K. M., & Zhu, Y. G. (2004). Relationships between soil characteristics, topography and plant diversity in a heterogeneous deciduous broad-leaved forest near Beijing, China. *Plant and Soil*, 261(1/2), 47–54. <https://doi.org/10.1023/B:PLSO.0000035567.97093.48>
- Guo, Y., Lu, J., Franklin, S. B., Wang, Q., Xu, Y., Zhang, K., et al. (2013). Spatial distribution of tree species in a species-rich subtropical mountain forest in central China. *Canadian Journal of Forest Research*, 43(9), 826–835. <https://doi.org/10.1139/cjfr-2013-0084>
- He, D. (2016). Plant functional trait variation and community assembly: A case study in a subtropical evergreen forest (PhD thesis). Sun Yat-sen University.
- Jiang, Q., Li, Q., Wang, X., Wu, Y., Yang, X., & Liu, F. (2017). Estimation of soil organic carbon and total nitrogen in different soil layers using VNIR spectroscopy: Effects of spiking on model applicability. *Geoderma*, 293, 54–63. <https://doi.org/10.1016/j.geoderma.2017.01.030>
- Jiang, Y., Zhang, B., Wang, W., Li, B., Wu, Z., & Chu, C. (2020). Topography and plant community structure contribute to the spatial heterogeneity of soil respiration in a subtropical forest. *Science of the Total Environment*, 733, 139287. <https://doi.org/10.1016/j.scitotenv.2020.139287>
- Li, Q. (2016). *Spatial variation of soil C and N and their determinants in a subtropical evergreen and deciduous broad-leaved mixed forest in Mt. Badagongshan* (PhD thesis). Wuhan Botanical Garden, Chinese Academy of Sciences.
- Li, Q., Wang, X., Jiang, M., Wu, Y., Yang, X., Liao, C., & Liu, F. (2017). How environmental and vegetation factors affect spatial patterns of soil carbon and nitrogen in a subtropical mixed forest in Central China. *Journal of Soils and Sediments*, 17(9), 2296–2304. <https://doi.org/10.1007/s11368-016-1491-5>
- Liu, H., Li, L., & Sang, W. (2011). Species composition and community structure of the Donglingshan forest dynamic plot in a warm temperate deciduous broad-leaved secondary forest, China. *Biodiversity Science*, 19(2), 232–242. (In Chinese with English abstract). <https://doi.org/10.3724/SP.J.1003.2011.11319>
- Liu, R., Zhou, X., Wang, J., Shao, J., Fu, Y., Liang, C., et al. (2019). Differential magnitude of rhizosphere effects on soil aggregation at three stages of subtropical secondary forest successions. *Plant and Soil*, 436(1–2), 365–380. <https://doi.org/10.1007/s11104-019-03935-z>
- Liang, M., Liu, X., Parker, I. M., Johnson, D., Zheng, Y., Luo, S., et al. (2019). Soil microbes drive phylogenetic diversity-productivity relationships in a subtropical forest. *Science Advances*, 5(10), eaax5088. <https://doi.org/10.1126/sciadv.aax5088>
- Liang, X., Liu, S., Wang, H., & Wang, J. (2018). Variation of carbon and nitrogen stoichiometry along a chronosequence of natural temperate forest in northeastern China. *Journal of Plant Ecology*, 11(3), 339–350. <https://doi.org/10.1093/jpe/rtx008>
- Qiao, X., Li, Q., Jiang, Q., Lu, J., Franklin, S., Tang, Z., et al. (2015). Beta diversity determinants in Badagongshan, a subtropical forest in central China. *Scientific Reports*, 5, 1–9. <https://doi.org/10.1038/srep17043>
- Wang, J., Yang, Q., Qiao, Y., Zhai, D., Jiang, L., Liang, G., et al. (2019). Relative contributions of biotic and abiotic factors to the spatial variation of litter stock in a mature subtropical forest. *Journal of Plant Ecology*, 12(4), 769–780. <https://doi.org/10.1093/jpe/rtz018>
- Xie, X., Wang, Q., Dai, L., Su, D., Wang, X., Qi, G., & Ye, Y. (2011). Application of China's National Forest Continuous Inventory Database. *Environmental Management*, 48(6), 1095–1106. <https://doi.org/10.1007/s00267-011-9716-2>

- Yan, E. R., Wang, X. H., Guo, M., Zhong, Q., Zhou, W., & Li, Y. F. (2009). Temporal patterns of net soil N mineralization and nitrification through secondary succession in the subtropical forests of eastern China. *Plant and Soil*, 320(1–2), 181–194. <https://doi.org/10.1007/s11104-008-9883-y>
- Zhao, H. C., Gao, F., Li, S. W., Gao, L., Wang, M. Z., & Cui, X. Y. (2019). Co-accumulation characters of organic carbon and nitrogen under broadleaved Korean pine and *Betula Platyphylla* secondary forests in Changbai Mountain, China. *Chinese Journal of Applied Ecology*, 30, 1615–1624. (In Chinese with English abstract). <https://doi.org/10.13287/j.1001-9332.201905.040>
- Zhang, R.-H. (2015). Natural and human-induced changes in summer climate over the East Asian monsoon region in the last half-century: A review. *Advances in Climate Change Research*, 6(2), 131–140. <https://doi.org/10.1016/j.accre.2015.09.009>
- Zhang, Y., Yao, Y., Wang, X., Liu, Y., & Piao, S. (2017). Mapping spatial distribution of forest age in China. *Earth and Space Science*, 4(3), 108–116. <https://doi.org/10.1002/2016EA000177>